THE JOURNAL OF PHYSICAL CHEMISTRY Letters

Letter

pubs.acs.org/JPCL

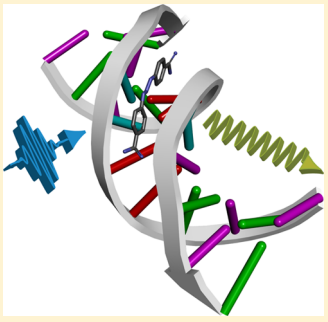
Ultrafast Dynamics of a Triazene: Excited-State Pathways and the Impact of Binding to the Minor Groove of DNA and Further Biomolecular Systems

Lena Grimmelsmann,[†] Alireza Marefat Khah,[‡] Christian Spies,[†] Christof Hättig,*[,‡] and Patrick Nuernberger*[,†]

[†]Physikalische Chemie II and [‡]Theoretische Chemie, Ruhr-Universität Bochum, 44780 Bochum, Germany

Supporting Information

ABSTRACT: Many synthetic DNA minor groove binders exhibit a strong increase in fluorescence when bound to DNA. The pharmaceutical-relevant berenil (diminazene aceturate) is an exception with an extremely low fluorescence quantum yield (on the order of 10^{-4}). We investigate the ultrafast excited-state dynamics of this triazene by femtosecond time-resolved fluorescence experiments in water, ethylene glycol, and buffer and bound to the enzyme β-trypsin, the minor groove of AT-rich DNA, and G-quadruplex DNA. Ab initio calculations provide additional mechanistic insight. The complementing studies unveil that the excited-state motion initiated by $\pi\pi^*$ excitation occurs in two phases: a subpicosecond phase associated with the lengthening of the central N═N double bond, followed by a bicycle-pedal-type motion of the triazene bridge, which is almost volume-conserving and can proceed efficiently within only a few picoseconds even under spatially confined conditions. Our results elucidate the excited-state relaxation mechanism of aromatic triazenes and explain the modest sensitivity of the fluorescence quantum yield of berenil even when it is bound to various biomolecules.



Downloaded via BOCHUM LIBRARIES on January 16, 2019 at 09:28:57 (UTC).
See https://pubs.acs.org/sharingguidelines for options on how to legitimately share published articles.

Triazene compounds are employed for a variety of medical and pharmaceutical applications. For instance, berenil is the most widely used drug for treating sleeping sickness in animals, and it also acts as babesiacide.[1−6] However, little is known about the underlying mechanism and how the properties of berenil change upon interaction with biomolecules. Berenil shows a high binding affinity to enzymes like β-trypsin[7,8] or diamine oxidase,[9] it is an efficient minor-groove binder of AT-rich DNA,[1,10−20] and it also strongly binds to G-quadruplex DNA.[21,22] A characteristic blue fluorescence emitted by berenil after UV excitation is observable when it is added to cell cultures that are in the stationary or lag phase of a growth cycle, yet it is absent when berenil is added to cells in the log phase.[1,23] Until now, no explanation could be found for this exceptional behavior, and, in general, emission from berenil is not reported but the molecule is rather described as nonfluorescent.[16,24] While these observations suggest that the deactivation channel of berenil after photoexcitation is sensitive to the surrounding, the virtual absence of fluorescence hints to very fast excited-state dynamics comprising photoisomerization and internal conversion.

Berenil (diminazene aceturate) is composed of two amidinophenyl units linked by a triazene bridge (Figure 1). It has some similarities to azobenzene in which two phenyl rings are linked by an azo group. The abilities to bind to biomolecules are very different for azobenzene and berenil, the latter being more flexible and exhibiting more possibilities for hydrogen-bond and electrostatic interactions due to the charged terminal groups. Regarding the photodynamics, despite numerous papers on the behavior of azobenzene after excitation, there is still an ongoing debate considering its photochemistry.[25−30] The reaction mechanisms discussed for its photoisomerization include inversion, rotation, the hula-twist,[30] and the concerted double twist.[31,32] By contrast, the triazene bridge in berenil contains an amino (NH) group in addition to the azo bond, which increases the number of torsional angles that can be involved in the excited-state relaxation. This opens alternative pathways for deactivation.

To unravel the mechanism of the ultrafast excited-state dynamics of berenil, we combine ultrafast fluorescence upconversion measurements of berenil bound to large biomolecules or in solvents with different viscosity with correlated wave function calculations for the potential energy surface of the excited state. In this way, the ultrafast deactivation and the extremely low fluorescence quantum yield found for all of these conditions can be rationalized.

Steady-state absorption and emission spectra of berenil in buffer (50 mM Tris-HCl, 250 mM KCl) are shown in Figure 1. The absorption maximum is located at 368 nm with an extinction coefficient of (26 500 ± 2300) M^{-1} cm^{-1}.[33] The fluorescence exhibits a large Stokes shift and peaks at 476 nm and is extremely weak, as confirmed by the low quantum yield of 0.9×10^{-4} that we derived in a Strickler−Berg analysis[34] with several reference substances for consistency.

Received: February 27, 2017
Accepted: April 13, 2017
Published: April 20, 2017

 © 2017 American Chemical Society

DOI: 10.1021/acs.jpclett.7b00472
J. Phys. Chem. Lett. 2017, 8, 1986−1992

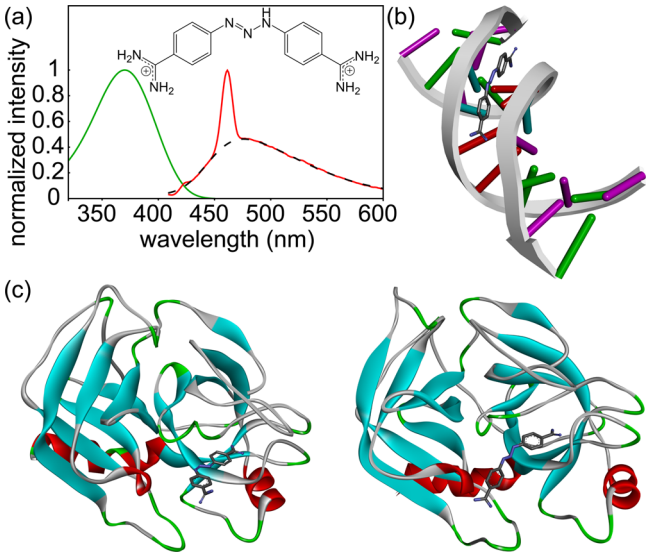


Figure 1. (a) Chemical structure of berenil and its absorption (green) and emission spectrum (red, excited at 400 nm) in buffer solution. Because of the low fluorescence quantum yield, Raman scattering in the solvent contributes as a pronounced peak at 462 nm. The dashed line is the Raman-corrected emission, as employed for the Strickler–Berg analysis. Cartoon representation of berenil bound to (b) AT-rich DNA (PDB accession code 2DBE)[13] and to (c) β-trypsin (left: 3GY6; right: 3GY2).[8]

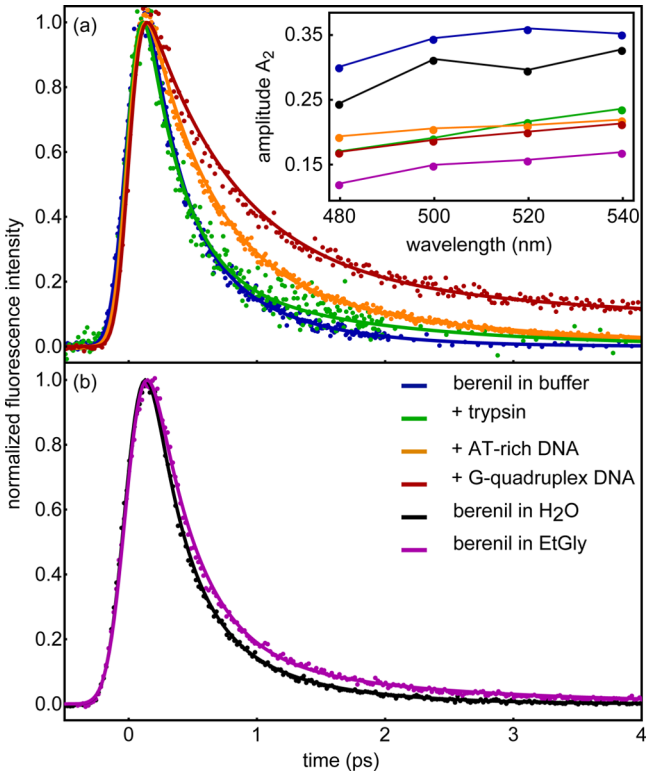


Figure 2. Transient fluorescence signal of berenil at an emission wavelength of 480 nm. (a) In Tris-HCl and the corresponding salt (in the case of unbound berenil and bound to the DNAs: KCl; in the case of berenil bound to trypsin: $CaCl_2$): unbound (blue), bound to trypsin (green), bound to AT-rich DNA (orange), and bound to G-quadruplex DNA (red). (b) In water (black) and ethylene glycol (magenta). Dots show data points, while lines are results from global fitting. The inset at the top-right shows the relative amplitude A_2 of the long lifetime in these fits as a function of fluorescence wavelength.

As biomolecular binding partners, we studied β-trypsin, AT-rich DNA (sequence 5′ to 3′: CGAATTTCAAAAGAAATT-CG), and G-quadruplex DNA (AGGGAGGGCGCTGGG-AGGAGGG) because of the reported high binding affinity of berenil to these kinds of biomolecules.[7,8,13,21] The binding between the particular system and berenil is reflected in characteristic shifts[10] in the absorption spectra (Figure S2 in the Supporting Information). Time-resolved fluorescence spectroscopy (see Supporting Information for experimental details) provides insight into the decay behavior, as shown in Figure 2 for berenil in buffer solution and bound to the different biomolecules as well as in neat water and ethylene glycol, respectively. Only results for an emission wavelength of 480 nm are shown for a direct comparison (best-fit parameter values with error limits are summarized in Table 1); data and fits for other wavelengths are presented in the SI. In each case, the best global deconvolution fit for all measured samples yields two lifetimes. For the buffer solution (blue curve), global decay times of 0.24 and 0.71 ps are found, and the amplitude A_2 of the second lifetime increases with increasing fluorescence wavelength (amplitude ratio 70:30 at 480 nm, 65:35 at 540 nm, inset of Figure 2).

When berenil is bound to β-trypsin, two main structures are present with berenil in different conformations (Figure 1c), and several hydrogen bonds between one of the amidinium groups and the protein are formed, while further interactions are possible.[8] Nevertheless, the two fitted lifetimes are only slightly increased to 0.28 and 1.41 ps. The amplitude of the latter again increases with wavelength (83:17 at 480 nm, 76:24 at 540 nm, inset of Figure 2).

For berenil bound to AT-rich DNA (Figure 1b), one amidinium moiety hydrogen-bonds directly to an adenine base, whereas the other one interacts with the DNA via a mediating water molecule.[13] This binding to the DNA minor groove restricts the volume available for geometrical changes of berenil, which should be even more confined when berenil is bound to the G-quadruplex DNA. Looking at the decay traces of berenil bound to the DNAs, the traces clearly deviate from the one of berenil in buffer only. The corresponding lifetimes are 0.48 and 1.77 ps for berenil bound to AT-rich DNA (orange line) and 0.69 and 6.55 ps for G-quadruplex DNA (red line), respectively. By analogy to the cases with buffer only and binding to β-trypsin, the amplitude A_2 increases with increasing wavelength (81:19 at 480 nm, 78:22 for 540 nm and 83:17 at 480 nm, 79:21 for 540 nm, respectively, inset of Figure 2). When calculating amplitude-weighted lifetimes τ_{ave} (Table 1), the general trend is the same as for the individual time constants: While τ_{ave} is 0.38 ps for berenil in buffer, it is larger for berenil bound to trypsin (0.47 ps) and to AT-rich DNA (0.73 ps). With 1.69 ps, the largest τ_{ave} value is found for berenil bound to G-quadruplex DNA.

These results are in opposition to the behavior of another efficient DNA binder, DAPI, for which the fluorescence lifetime is enhanced from 100 ps for DAPI dissolved in buffer to several nanoseconds when DAPI is bound to the minor groove of a DNA dodecamer.[35] Compared with this, the lifetime prolongation we observe for berenil is rather small. To further explore if the reason for this is the expendability of large geometrical changes after photoexcitation, we studied berenil in two solvents with different viscosity. The lifetimes for berenil in neat water (0.25 and 0.73 ps) are basically identical to the ones obtained for berenil in Tris-HCl and KCl buffered solution. In

DOI: 10.1021/acs.jpclett.7b00472
J. Phys. Chem. Lett. 2017, 8, 1986−1992

Table 1. Time Constants Obtained by Global Fitting of the Fluorescence Upconversion Data[a]

sample	A_1	τ_1 (ps)	A_2	τ_2 (ps)	τ_{ave} (ps)
berenil in buffer	0.70 ± 0.07	0.24 ± 0.03	0.30 ± 0.07	0.71 ± 0.08	0.38 ± 0.06
berenil + trypsin	0.83 ± 0.04	0.28 ± 0.02	0.17 ± 0.04	1.41 ± 0.24	0.47 ± 0.07
berenil + AT-rich DNA	0.81 ± 0.01	0.48 ± 0.01	0.19 ± 0.01	1.77 ± 0.08	0.73 ± 0.03
berenil + G-quad. DNA	0.83 ± 0.01	0.69 ± 0.02	0.17 ± 0.01	6.55 ± 0.52	1.69 ± 0.11
berenil in water	0.75 ± 0.03	0.25 ± 0.01	0.25 ± 0.03	0.73 ± 0.03	0.37 ± 0.03
berenil in ethylene glycol	0.88 ± 0.01	0.34 ± 0.01	0.12 ± 0.01	1.57 ± 0.08	0.49 ± 0.02

[a]Relative amplitudes and amplitude-weighted average fluorescence lifetimes correspond to an emission wavelength of 480 nm (i.e., the data displayed in Figure 2; see Table S2 in the Supporting Information for other emission wavelengths).

ethylene glycol, the lifetimes are only slightly extended (0.34 and 1.57 ps), and, remarkably, the amplitude A_2 takes the lowest values with the same overall trend of an increase with wavelength (88:12 at 480 nm, 83:17 at 540 nm, inset of Figure 2), which is reflected in the rather small increase in τ_{ave} from 0.37 to 0.49 ps (Table 1). The viscosity of ethylene glycol (20.8 mPa·s at 20 °C)[36] is ∼20 times higher than the viscosity of water (1.00 mPa·s at 20 °C).[36] In numerous studies where deactivation follows a cis−trans isomerization by rotation around a C═C bond, changing the solvent viscosity leads to a significant increase in the fluorescence lifetime.[37−41] The rather weak dependence of the fluorescence lifetime of berenil on the solvent viscosity leads to analogous implications as the studies with berenil bound to biomolecules, namely, that a very fast nonradiative deactivation mechanism must be involved that cannot be associated with pronounced intramolecular motion.

If the deactivation proceeded via rotation, the fluorescence lifetimes should be significantly enhanced when changing the viscosity of the solvent. Therefore, we exclude the rotation as a possible deactivation channel. An in-plane motion of the phenyl rings as for the inversion mechanism is expected to be less affected by a higher viscosity. When berenil is bound to trypsin or DNA the volume accessible for the molecule should be substantially smaller than that for unbound berenil. Therefore, the time needed for deactivating structural dynamics along the inversion mechanism would still be expected to be longer for bound berenil. The associated enhancement of the emission lifetimes is deducible from the decay traces. However, the time-resolved fluorescence studies disclose that there is only a slight prolongation, which argues against deactivation pathways with predominant character of rotation and inversion.[31,42−44] Consequently, we also exclude inversion as deactivation mechanism.

To get further insight into the absorption and fluorescence spectra, we used ab initio electronic structure calculations. Under the experimental and also physiological conditions[18,20] diminazene is doubly protonated. Using dispersion-corrected density functional theory (DFT-D3) for geometry optimizations, we could characterize six local minima on the electronic ground-state potential energy surface of the doubly protonated diminazene as pairs with "*E-azo*, *s-trans*" (ET), "*E-azo*, *s-cis*" (EC), and "*Z-azo*, *s-trans*" (ZT) structure. The details of the computational procedure as well as the molecular structures of all conformers are available in the Supporting Information. Second-order Møller−Plesset perturbation theory (RI-MP2) has been used to obtain accurate relative energies. According to these results, at room temperature in the thermodynamic equilibrium only the ET minima are significantly occupied. Characteristic for the *E-azo* conformers is that the triazene bridge and the phenyl rings are coplanar and the amidinium groups are twisted by ∼30° either dis- or conrotatory out of this plane.

The energies and oscillator strengths for the five lowest excited states of the ET conformers have been calculated with the algebraic diagrammatic construction through second order,[45,46] ADC(2), in vacuum and with the COSMO solvation model[47,48] for aqueous solution (ε = 50) with the SVP and aug-cc-pVDZ basis sets (see Supporting Information). The results show that the relative orientation (dis- or conrotatory) of the amidinium groups has no influence on the spectrum. The excitation into S_1 is the only bright transition below 5 eV. The vertical excitation energy of 3.32 eV for the transition into S_1 computed at the COSMO-ADC(2)/aug-cc-pVDZ level agrees well with the first maximum in the experimental UV/vis spectrum at ∼3.35 eV (Figure 1a).[10,33] At the ground-state structure the transition to S_1 is dominated by a $\pi\pi^*$ excitation from an occupied natural transition orbital[49] (NTO), which has bonding character for the N═N azo bond (no nodal plane between these two nitrogen atoms) to a virtual NTO with antibonding character for the N═N bond (see Figure S6 in the Supporting Information). Consequently, the π bond between these N atoms is broken in the S_1 state. The C−N π bonds between the NH−N═N moiety and the benzene rings are strengthened in the S_1 state.

The results for the absorption spectrum in vacuum and in aqueous solution show only minor differences, that is, for the transition into S_1, a red shift by 0.02 eV and a decrease in the oscillator strength by ∼2%. Furthermore, in the smaller and computationally cheaper SVP basis set the excitation energies are only slightly blue-shifted, but the same orbitals are involved in the excitation to S_1, and thus it also describes the electronic structure of S_1 correctly. Because neither the excitation energy nor the oscillator strengths depend on the orientation of the $-C(NH_2)_2$ groups, we have chosen one of the ET conformers (the $ET1_{S0}$ structure in Figure 3) and the ADC(2)/SVP level of theory without COSMO to investigate the relaxation of the photoactivated molecule.

For the S_1 state, we found two local minima denoted as $ET1_{S1}$ and $ET1_{RS1}$, which can be reached from the Franck−Condon point after excitation. Their structures, which differ from the ground-state geometry by clockwise ($ET1_{RS1}$) and anticlockwise ($ET1_{S1}$) torsion around the azo bond, are shown in Figure 3. The two minima on the S_1 surface are connected by a transition state, $ET1_{TS-S1}$, which differs from the ground-state structure mainly by a stretch of the azo bond. At the $ET1_{S1}$ and $ET1_{RS1}$ geometries the COSMO-ADC(2)/aug-cc-pVDZ energy of the S_1 state is slightly below the COSMO-RI-MP2/aug-cc-pVDZ energy of S_0. This indicates that in these regions the two states might be connected by conical intersections.

To investigate the deactivation pathways, we carried out intrinsic reaction coordinate (IRC) calculations at the

DOI: 10.1021/acs.jpclett.7b00472
J. Phys. Chem. Lett. 2017, 8, 1986−1992

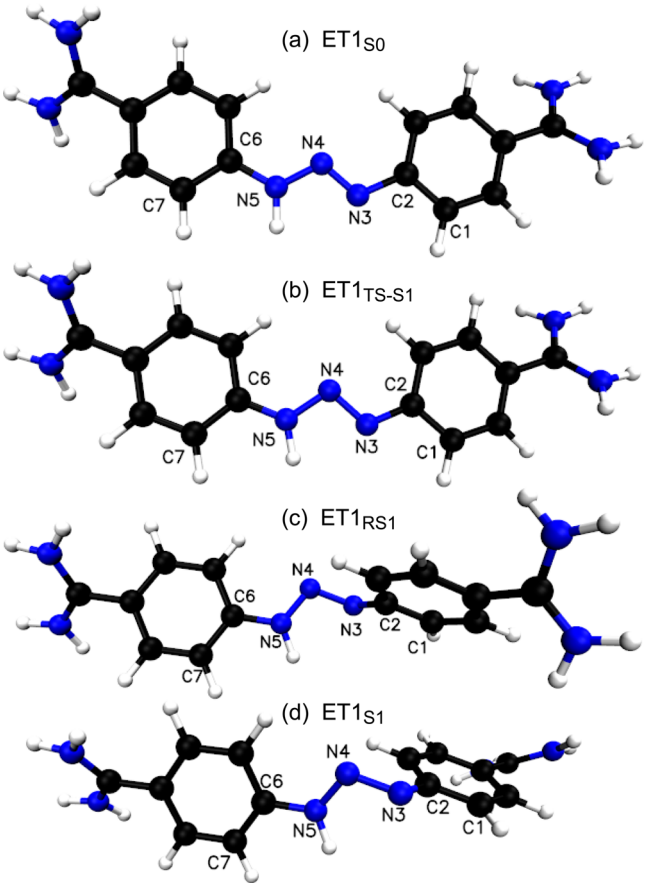


Figure 3. Optimized stationary points for the ground state and the lowest excited state at the ADC(2)/SVP level of theory. At the transition state $ET1_{TS-S1}$, the phenyl groups are almost coplanar while at the minima $ET1_{S1}$ and $ET1_{RS1}$ they are twisted by ~90° around the N_3═N_4 bond anticlockwise and clockwise, respectively.

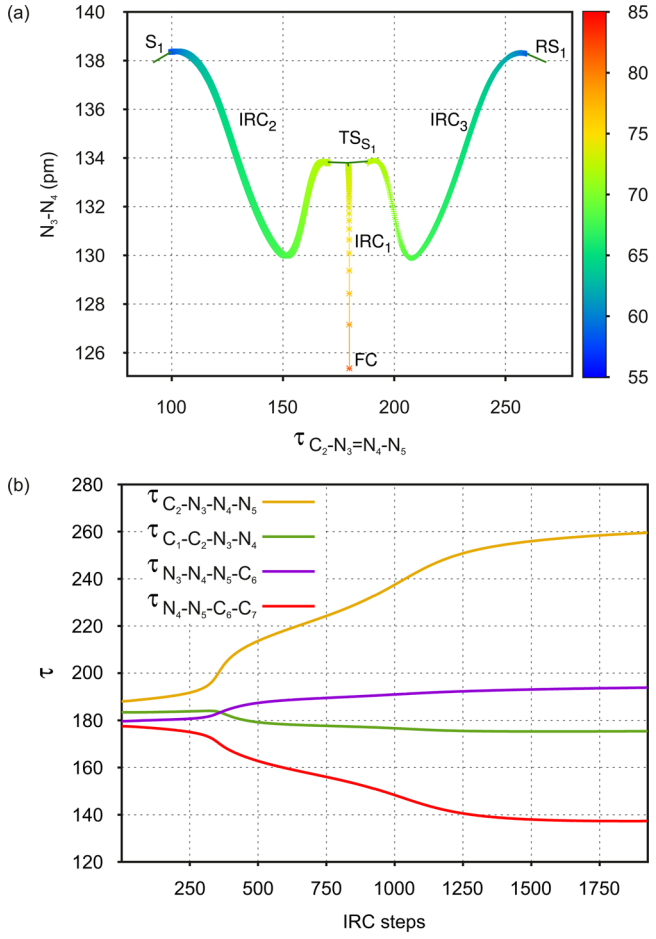


Figure 4. (a) Calculated (ADC(2)/RI-MP2)/SVP intrinsic reaction coordinates are mapped to the N_3═N_4 double bond and the C_2–N_3–N_4–N_5 dihedral angle. The Figure presents the results of three independent IRC calculations. Colors indicate for each point the energy relative to the ground state at $ET1_{S1}$ in kcal·mol^{-1}. The IRC_1 starts from the FC point. The IRC_2 starts from the ~−10° screwed TS_{S1} geometry along the normal mode with imaginary frequency and the IRC_3 from the ~+10° rotated TS_{S1} geometry. The green lines connect the starting and ending point of the IRC calculations to the corresponding stationary points. (b) Evolution of triazene dihedral angles along the IRC_3 trajectory.

ADC(2)/SVP level on the S_1 surface starting from the Franck–Condon point. The idea of the IRC analysis is to calculate nuclear gradients at a given geometry, let the nuclei move for a certain time step δt (= 2 fs in this case) according to Newton's second law, and again calculate the gradients and a geometry update for the new coordinates until a stationary point is reached where the gradients are zero within a given threshold. In the IRC analysis,[50,51] the kinetic energy is at each step damped to zero to follow the minimum energy reaction pathway.[52]

Figure 4a shows how the two most important internal coordinates, the length of the N_3═N_4 azo bond and the C_2–N_3═N_4–N_5 dihedral angle, change along the IRC trajectories. The density of the points can be interpreted as the inverse of the gradient (force) norm along the internal coordinates. This Figure shows that the first phase (IRC_1) of the de-excitation is a fast departure from the Franck–Condon region, which is characterized by a N_3═N_4 bond stretch and brings the molecules to a flat region on the S_1 surface. An optimization starting from the end point of the IRC_1 path led to the transition state $ET1_{TS-S1}$, which is very similar to the last snapshot of the IRC_1 calculation. To continue the IRC calculations, the TS_{S1} geometry has been screwed along the normal mode with negative eigenvalue for ~±10°. The obtained paths (IRC_2 and IRC_3) show that the second phase of the de-excitation involves a torsion of the C_2–N_3═N_4–N_5 dihedral angle. The two pathways lead to the two minima $ET1_{S1}$ and $ET1_{RS1}$ on the S_1 surface described above (Figure 3).

The two clockwise and anticlockwise rotation paths are similar to each other and involve, in addition to changes of the length and torsion angle of the azo bond, torsions around other bonds at the triazene group. To further unravel the mechanism of the second de-excitation phase, Figure 4b shows the four dihedral angles at the triazene group along the IRC_3 path. Several mechanisms have been discussed in the literature for the (photo)isomerization of chromophores with double bonds. The most important ones are the pure torsion rotation, the Hula-twist mechanism,[43,53] in-plane inversion, concerted double-twist,[31] and the bicycle-pedal type mechanism.[44,54] The moderate sensitivity of the deactivation dynamics to the viscosity of the solvent observed in the experiments already ruled out inversion and rotation as relaxation mechanisms.

The Hula-twist mechanism would for berenil imply simultaneous torsions around the N_3N_4 and N_4N_5 (or C_2N_3) bonds with about the same amplitude, whereas the concerted

DOI: 10.1021/acs.jpclett.7b00472
J. Phys. Chem. Lett. 2017, 8, 1986–1992

double-twist mechanism is identified with concerted out-of-plane motion of $N_3{=}N_4$ nitrogens—here the simultaneous rotation around C_2N_3, N_3N_4 and N_4N_5 bonds. According to Figure 4b, the molecule rotates by ∼70° around the N_3N_4 bond but only by ∼20° around the N_4N_5 and C_2N_3 bonds. Consequently, neither the Hula-twist nor the concerted double twist are the mechanisms of the second phase. The torsion around the azo bond is accompanied by a simultaneous rotation around the N_5C_6 bond by ∼40°. Although the amplitude of the latter motion is somewhat smaller than for the torsion around the azo bond, it is by far the most important component of the torsional motions next to the torsion around the azo bond. Thus we conclude that the relaxation mechanism is predominantly a bicycle-pedal type motion, which is almost volume-conserving.[44,55] This explains the fast radiationless de-excitation in solution and with various biomolecular binding partners because it does not require large amplitude motions of the terminal phenyl and amidinium groups.

While no indication for an intersystem crossing is evident from our data or from the literature, the ultrafast fluorescence decay is attributed to ultrafast geometrical changes, rapidly leading to internal conversion back to the electronic ground state. From several possibilities for this structural motion, the combined information from experiment and theory allows for an unambiguous identification. A rotation of the phenol's sidegroup,[56] that is, the amidinium groups, after photo-excitation can be ruled out as decisive process for two reasons: On the one hand, this motion would be hindered when berenil is hydrogen-bonded to the biomolecules, yet the dynamics do not change drastically, in contrast with the minor-groove binder DAPI where this mechanism is known to contribute to the relaxation[35] and hence causes an enhancement of emission lifetimes by more than an order of magnitude; on the other hand, our simulations show that these motions are not the favorable mechanism for the relaxation from the Franck–Condon point on the excited-state potential energy surface.

Hence, the triazene bridge is crucially involved in the de-excitation but in a way that is different from a cis–trans isomerization found for compounds with C=C double bonds,[37−41] as can be deduced from the experimentally observed viscosity dependence. To clarify the structural dynamics of the triazene bridge, we can first address similarities to the dynamics of azobenzene, for which also two lifetimes were found in the fluorescence decay traces. Quick et al.[30] assigned the 0.3 ps lifetime of *trans*-azobenzene to a rapid motion away from the Franck–Condon region to a local minimum, while the longer lifetime of 3 ps was attributed to a population relaxation. This rather slow population relaxation in the excited state is associated with a barrier of 8 kJ/mol.

In the case of berenil, the short lifetime is in the range between 0.24 ps for unbound berenil and 0.69 ps for berenil bound to G-quadruplex DNA. They match well the first fluorescence lifetime of azobenzene and can be interpreted accordingly. As is evident from the simulations and the IRC_1 path in Figure 4a, the initial motion setting in after photoexcitation and concurrent cleavage of the N=N π-bond in the S_1 state is a lengthening of the N=N bond distance, which is accompanied by a change of the oscillator strength. These dynamics are experimentally monitored by the rapidly decaying fluorescence contribution; that is, the first lifetime reflects the motion out of the Franck–Condon region. Albeit slight prolongations are observed, the first lifetime is much less affected by the different confining conditions than is the second one, which spans an order of magnitude from 0.71 ps for unbound berenil to 6.55 ps for berenil bound to G-quadruplex DNA. Hence the experiments imply that relaxation occurs in two phases associated with two different types of motion.

This finding is supported by the calculations at the ADC(2) level. The computational investigations of the relaxation from the Franck–Condon point to the minima on the S_1 surface show the two relaxation phases. Initially, the molecule approaches a transition state where the azo bond is stretched but the triazene and phenyl groups are still coplanar. Through this first phase, 16.1 kcal·mol^{-1} of the absorbed energy is released. The second phase is dominated by a bicycle-pedal type motion around the $N_3{=}N_4$ and $N_5{-}C_6$ bonds that links the transition state TS_{S_1} to the two minima (S_1 and R–S_1) on the S_1 surface, depending on the direction of the torsional motion. Also, the second phase of the relaxation is strongly exothermic and releases ∼19.4 kcal·mol^{-1} energy. Similar to the first phase, this step requires no large amplitude motions of the bulky groups. The fluorescence exhibits an initial red shift. We do not observe (or possibly resolve) a dynamic Stokes shift starting at the excitation wavelength with a delayed onset of long-wavelength emission, as may be caused by solvent reorganization or intramolecular vibrational relaxation. Nevertheless, the spectral composition of the fluorescence contains valuable information. Around the S_1 and R–S_1 regions, the energy gap between S_0 and S_1 is small, and the two states are probably connected via conical intersections. Hence, the central fluorescence wavelength should be different for the two relaxation phases as a consequence of the shrinking energy gap when following the IRC_2 and IRC_3 reaction paths. Hence, the associated release of energy during relaxation is manifested in the relative amplitudes of the fluorescence decays. The inset of Figure 2 displays an increasing relative amplitude of the longer lifetime with increasing emission wavelength; that is, the emission corresponding to the second relaxation phase is spectrally centered at lower energy photons.

In summary, the joint experimental and theoretical study shows that the efficient minor-groove binder berenil performs an ultrafast motion in the electronically excited state after $\pi\pi^*$ excitation. The dynamics comprise two phases: first, a contribution out of the Franck–Condon region associated with the lengthening of the initial N=N double bond and a subsequent bicycle-pedal type motion of the central triazene unit. Time-resolved fluorescence studies of berenil in water, buffer, or ethylene glycol and bound to β-trypsin, AT-rich DNA, or G-quadruplex DNA revealed that the first phase proceeds on a subpicosecond time scale, whereas the second phase still occurs within only a few picoseconds for all of the investigated conditions despite several hydrogen bonds or different spatial restrictions. The volume-conserving nature of the bicycle-pedal type motion renders possible extremely fast excited-state dynamics in berenil and thus explains the very low fluorescence quantum yield and the frequently encountered classification of berenil as being "nonfluorescent".

■ ASSOCIATED CONTENT

Supporting Information

The Supporting Information is available free of charge on the ACS Publications website at DOI: 10.1021/acs.jpclett.7b00472.

Details of sample preparation, experimental procedures, absorption/emission spectra, and transient fluorescence

DOI: 10.1021/acs.jpclett.7b00472
J. Phys. Chem. Lett. 2017, 8, 1986−1992

signals for all samples, computational details, optimized structures.(PDF)

AUTHOR INFORMATION

Corresponding Authors

*C.H.: E-mail: christof.haettig@rub.de.

*P.N.: E-mail: patrick.nuernberger@rub.de.

ORCID

Patrick Nuernberger: 0000-0002-4690-0229

Notes

The authors declare no competing financial interest.

ACKNOWLEDGMENTS

We are grateful to Prof. Christian Herrmann and Prof. Lars Schäfer for helpful discussions and to Bastian Geißler for assistance with global fitting. This work has been supported by the Deutsche Forschungsgemeinschaft within the Cluster of Excellence RESOLV (EXC 1069) and the Emmy-Noether program (PN).

REFERENCES

(1) Newton, B. A. Berenil: A trypanocide with selective activity against extranuclear DNA. In *Mechanism of Action of Antimicrobial and Antitumor Agents*; Corcoran, J. W., Hahn, F. E., Snell, J. F., Arora, K. L., Eds.; Springer: Berlin, Germany, 1975; pp 34−47.

(2) Peregrine, A. S.; Mamman, M. Pharmacology of diminazene. *Acta Trop.* **1993**, *54*, 185−203.

(3) Khaw, M.; Panosian, C. B. Human antiprotozoal therapy: Past, present, and future. *Clin. Microbiol. Rev.* **1995**, *8*, 427−439.

(4) Kuriakose, S.; Muleme, H. M.; Onyilagha, C.; Singh, R.; Jia, P.; Uzonna, J. E. Diminazene aceturate (berenil) modulates the host cellular and inflammatory responses to trypanosoma congolense infection. *PLoS One* **2012**, *7*, e48696.

(5) Kuriakose, S.; Uzonna, J. E. Diminazene aceturate (berenil), a new use for an old compound? *Int. Immunopharmacol.* **2014**, *21*, 342−345.

(6) da Silva Oliveira, G. L.; de Freitas, R. M. Diminazene aceturate−An antiparasitic drug of antiquity: Advances in pharmacology & therapeutics. *Pharmacol. Res.* **2015**, *102*, 138−157.

(7) Pereira, M. T.; Silva-Alves, J. M.; Martins-Jose, A.; Lopes, J. C. D.; Santoro, M. M. Thermodynamic evaluation and modeling of proton and water exchange associated with benzamidine and berenil binding to ß-trypsin. *Braz. J. Med. Biol. Res.* **2005**, *38*, 1593−1601.

(8) Perilo, C. S.; Pereira, M. T.; Santoro, M. M.; Nagem, R. A. P. Structural binding evidence of the trypanocidal drugs Berenil and Pentacarinate active principles to a serine protease model. *Int. J. Biol. Macromol.* **2010**, *46*, 502−511.

(9) McGrath, A. P.; Hilmer, K. M.; Collyer, C. A.; Shepard, E. M.; Elmore, B. O.; Brown, D. E.; Dooley, D. M.; Guss, J. M. Structure and inhibition of human diamine oxidase. *Biochemistry* **2009**, *48*, 9810−9822.

(10) Festy, B.; Lallemant, A.-M.; Riou, G.; Brack, C.; Delain, E. Mécanisme d'action des diamidines trypanocides. Importance de la composition en bases dans l'association berenil-polynucléotides. *C. R. Hebd. Séances Acad. Sci. D* **1970**, *271*, 684−687.

(11) Zimmer, C.; Wähnert, U. Nonintercalating DNA-binding ligands: Specificity of the interaction and their use as tools in biophysical, biochemical and biological investigations of the genetic material. *Prog. Biophys. Mol. Biol.* **1986**, *47*, 31−112.

(12) Yoshida, M.; Banville, D. L.; Shafer, R. H. Structural analysis of $d(GCAATTGC)_2$ and its complex with berenil by nuclear magnetic resonance spectroscopy. *Biochemistry* **1990**, *29*, 6585−6592.

(13) Brown, D. G.; Sanderson, M. R.; Skelly, J. V.; Jenkins, T. C.; Brown, T.; Garman, E.; Stuart, D. I.; Neidle, S. Crystal structure of a berenil-dodecanucleotide complex: the role of water in sequence-specific ligand binding. *EMBO J.* **1990**, *9*, 1329−1334.

(14) Jenkins, T. C.; Lane, A. N.; Neidle, S.; Brown, D. G. NMR and molecular modeling studies of the interaction of berenil and pentamidine with $d(CGCAAATTTGCG)_2$. *Eur. J. Biochem.* **1993**, *213*, 1175−1184.

(15) Barceló, F.; Portugal, J. Berenil recognizes and changes the characteristics of adenine and thymine polynucleotide structures. *Biophys. Chem.* **1993**, *47*, 251−260.

(16) Pilch, D. S.; Kirolos, M. A.; Liu, X.; Plum, G. E.; Breslauer, K. J. Berenil [1,3-bis(4′-amidinophenyl)triazene] binding to DNA duplexes and to a RNA duplex: Evidence for both intercalative and minor groove binding properties. *Biochemistry* **1995**, *34*, 9962−9976.

(17) Tabernero, L.; Bella, J.; Alemán, C. Hydrogen bond geometry in DNA-minor groove binding drug complexes. *Nucleic Acids Res.* **1996**, *24*, 3458−3466.

(18) Reddy, B. S. P.; Sondhi, S. M.; Lown, J. W. Synthetic DNA minor groove-binding drugs. *Pharmacol. Ther.* **1999**, *84*, 1−111.

(19) Mallena, S.; Lee, M. P. H.; Bailly, C.; Neidle, S.; Kumar, A.; Boykin, D. W.; Wilson, W. D. Thiophene-based diamidine forms a "super" AT binding minor groove agent. *J. Am. Chem. Soc.* **2004**, *126*, 13659−13669.

(20) Zsila, F. Glycosaminoglycans are potential pharmacological targets for classic DNA minor groove binder drugs berenil and pentamidine. *Phys. Chem. Chem. Phys.* **2015**, *17*, 24560−24565.

(21) Zhou, J.; Le, V.; Kalia, D.; Nakayama, S.; Mikek, C.; Lewis, E. A.; Sintim, H. O. Diminazene or berenil, a classic duplex minor groove binder, binds to G-quadruplexes with low nanomolar dissociation constants and the amidine groups are also critical for G-quadruplex binding. *Mol. BioSyst.* **2014**, *10*, 2724−2734.

(22) Wang, C.; Carter-Cooper, B.; Du, Y.; Zhou, J.; Saeed, M. A.; Liu, J.; Guo, M.; Roembke, B.; Mikek, C.; Lewis, E. A.; Lapidus, R. G.; Sintim, H. O. Alkyne-substituted diminazene as G-quadruplex binders with anticancer activities. *Eur. J. Med. Chem.* **2016**, *118*, 266−275.

(23) Stockert, J. C.; Del Castillo, P.; Llorente, A. R.; Rasskin, D. M.; Romero, J. B.; Gómez, A. New fluorescence reactions in DNA cytochemistry. 1. Microscopic and spectroscopic studies on nonrigid fluorochromes. *Anal. Quant. Cytol. Histol.* **1990**, *12*, 1−10.

(24) Gabelica, V.; Rosu, F.; De Pauw, E.; Antoine, R.; Tabarin, T.; Broyer, M.; Dugourd, P. Electron photodetachment dissociation of DNA anions with covalently or noncovalently bound chromophores. *J. Am. Soc. Mass Spectrom.* **2007**, *18*, 1990−2000.

(25) Schultz, T.; Quenneville, J.; Levine, B.; Toniolo, A.; Martinez, T. J.; Lochbrunner, S.; Schmitt, M.; Shaffer, J. P.; Zgierski, M. Z.; Stolow, A. Mechanism and dynamics of azobenzene photoisomerization. *J. Am. Chem. Soc.* **2003**, *125*, 8098−8099.

(26) Satzger, H.; Spörlein, S.; Root, C.; Wachtveitl, J.; Zinth, W.; Gilch, P. Fluorescence spectra of trans- and cis-azobenzene-emission from the Franck-Condon State. *Chem. Phys. Lett.* **2003**, *372*, 216−223.

(27) Pancur, T.; Renth, F.; Temps, F.; Harbaum, B.; Krüger, A.; Herges, R.; Näther, C. Femtosecond fluorescence up-conversion spectroscopy of a rotation-restricted azobenzene after excitation to the S_1 state. *Phys. Chem. Chem. Phys.* **2005**, *7*, 1985−1989.

(28) Lu, Y.-C.; Diau, E. W.-G.; Rau, H. Femtosecond fluorescence dynamics of rotation-restricted azobenzenophanes: New evidence on the mechanism of trans→cis photoisomerization of azobenzene. *J. Phys. Chem. A* **2005**, *109*, 2090−2099.

(29) Bandara, H. M. D.; Burdette, S. C. Photoisomerization in different classes of azobenzene. *Chem. Soc. Rev.* **2012**, *41*, 1809−1825.

(30) Quick, M.; Dobryakov, A. L.; Gerecke, M.; Richter, C.; Berndt, F.; Ioffe, I. N.; Granovsky, A. A.; Mahrwald, R.; Ernsting, N. P.; Kovalenko, S. A. Photoisomerization dynamics and pathways of trans- and cis-azobenzenes in solution from broadband femtosecond spectroscopies and calculations. *J. Phys. Chem. B* **2014**, *118*, 8756−8771.

(31) Böckmann, M.; Doltsinis, N. L.; Marx, D. Enhanced photoswitching of bridged azobenzene studied by nonadiabatic ab initio simulation. *J. Chem. Phys.* **2012**, *137*, 22A505.

(32) Böckmann, M.; Braun, S.; Doltsinis, N. L.; Marx, D. Mimicking photoisomerisation of azo-materials by a force field switch derived from nonadiabatic ab initio simulations: Application to photo-

DOI: 10.1021/acs.jpclett.7b00472
J. Phys. Chem. Lett. 2017, 8, 1986−1992

switchable helical foldamers in solution. *J. Chem. Phys.* **2013**, *139*, 084108.
(33) Thünemann, A. F.; Schütt, D.; Sachse, R.; Schlaad, H.; Möhwald, H. Complexes of poly(ethylene oxide)-block-poly(L-glutamate) and diminazene. *Langmuir* **2006**, *22*, 2323−2328.
(34) Strickler, S. J.; Berg, R. A. Relationship between absorption intensity and fluorescence lifetime of molecules. *J. Chem. Phys.* **1962**, *37*, 814−822.
(35) Banerjee, D.; Pal, S. K. Dynamics in the DNA recognition by DAPI: Exploration of the various binding modes. *J. Phys. Chem. B* **2008**, *112*, 1016−1021.
(36) Tsierkezos, N. G.; Molinou, I. E. Thermodynamic properties of water + ethylene glycol at 283.15, 293.15, 303.15, and 313.15 K. *J. Chem. Eng. Data* **1998**, *43*, 989−993.
(37) Taylor, J. R.; Adams, M. C.; Sibbett, W. Investigation of viscosity dependent fluorescence lifetime using a synchronously operated picosecond streak camera. *Appl. Phys.* **1980**, *21*, 13−17.
(38) Bagchi, B.; Fleming, G. R.; Oxtoby, D. W. Theory of electronic relaxation in solution in the absence of an activation barrier. *J. Chem. Phys.* **1983**, *78*, 7375−7385.
(39) Åkesson, E.; Hakkarainen, A.; Laitinen, E.; Helenius, V.; Gillbro, T.; Korppi-Tommola, J.; Sundström, V. Analysis of microviscosity and reaction coordinate concepts in isomerization dynamics described by Kramers' Theory. *J. Chem. Phys.* **1991**, *95*, 6508−6523.
(40) Vauthey, E. Isomerisation dynamics of a thiacarbocyanine dye in different electronic states and in different classes of solvents. *Chem. Phys.* **1995**, *196*, 569−582.
(41) Vogt, G.; Nuernberger, P.; Gerber, G.; Improta, R.; Santoro, F. Femtosecond study on the isomerization dynamics of NK88. II. Excited-state dynamics. *J. Chem. Phys.* **2006**, *125*, 044513.
(42) Liu, R. S. H.; Asato, A. E. The primary process of vision and the structure of bathorhodopsin: A mechanism for photoisomerization of polyenes. *Proc. Natl. Acad. Sci. U. S. A.* **1985**, *82*, 259−263.
(43) Liu, R. S. H. Photoisomerization by Hula-Twist: A fundamental supramolecular photochemical reaction. *Acc. Chem. Res.* **2001**, *34*, 555−562.
(44) Schapiro, I.; Weingart, O.; Buss, V. Bicycle-pedal isomerization in a rhodopsin chromophore model. *J. Am. Chem. Soc.* **2009**, *131*, 16−17.
(45) Schirmer, J. Beyond the random-phase approximation: A new approximation scheme for the polarization propagator. *Phys. Rev. A: At., Mol., Opt. Phys.* **1982**, *26*, 2395−2416.
(46) Hättig, C. Structure optimizations for excited states with correlated second-order methods: CC2 and ADC(2). *Adv. Quantum Chem.* **2005**, *50*, 37−60.
(47) Klamt, A.; Schüürmann, G. COSMO: a new approach to dielectric screening in solvents with explicit expressions for the screening energy and its gradient. *J. Chem. Soc., Perkin Trans. 2* **1993**, *2*, 799−805.
(48) Lunkenheimer, B.; Köhn, A. Solvent effects on electronically excited states using the conductor-like screening model and the second-order correlated method ADC(2). *J. Chem. Theory Comput.* **2013**, *9*, 977−994.
(49) Martin, R. L. Natural transition orbitals. *J. Chem. Phys.* **2003**, *118*, 4775−4777.
(50) Fukui, K. A formulation of the reaction coordinate. *J. Phys. Chem.* **1970**, *74*, 4161−4163.
(51) Fukui, K. The path of chemical reactions - the IRC approach. *Acc. Chem. Res.* **1981**, *14*, 363−368.
(52) Hellweg, A. Heuristic control of kinetic energy in dynamic reaction coordinate calculations. *J. Comput. Chem.* **2013**, *34*, 1835−1841.
(53) Imamoto, Y.; Kuroda, T.; Kataoka, M.; Shevyakov, S.; Krishnamoorthy, G.; Liu, R. S. H. Photoisomerization by Hula Twist: 2,2′-dimethylstilbene and a ring-fused analogue. *Angew. Chem., Int. Ed.* **2003**, *42*, 3630−3633.
(54) Warshel, A. Bicycle-pedal model for the first step in the vision process. *Nature* **1976**, *260*, 679−683.
(55) Jung, Y. O.; Lee, J. H.; Kim, J.; Schmidt, M.; Moffat, K.; Šrajer, V.; Ihee, H. Volume-conserving trans-cis isomerization pathways in photoactive yellow protein visualized by picosecond X-ray crystallography. *Nat. Chem.* **2013**, *5*, 212−220.
(56) Kovalenko, S. A.; Schanz, R.; Farztdinov, V. M.; Hennig, H.; Ernsting, N. P. Femtosecond relaxation of photoexcited para-nitroaniline: solvation, charge transfer, internal conversion and cooling. *Chem. Phys. Lett.* **2000**, *323*, 312−322.

DOI: 10.1021/acs.jpclett.7b00472
J. Phys. Chem. Lett. 2017, 8, 1986−1992